

HELIOSEISMOLOGY WITH LONG RANGE DARK MATTER-BARYON INTERACTIONS

LÍDIO LOPES^{1,2,7}, PAOLO PANCI^{3,4,7}, JOSEPH SILK^{4,5,6,7}

(Dated: October 30, 2018)
Draft version October 30, 2018

ABSTRACT

Assuming the existence of a primordial asymmetry in the dark sector, we study how DM-baryon long-range interactions, induced by the kinetic mixing of a new $U(1)$ gauge boson and the photon, affects the evolution of the Sun and in turn the sound speed profile obtained from helioseismology. Thanks to the explicit dependence on the exchanged momenta in the differential cross section (Rutherford-like scattering), we find that dark matter particles with a mass of ~ 10 GeV, kinetic mixing parameter of the order of 10^{-9} and a mediator with a mass smaller than a few MeV improve the agreement between the best solar model and the helioseismic data without being excluded by direct detection experiments. In particular, the LUX detector will soon be able to either constrain or confirm our best fit solar model in the presence of a dark sector with long-range interactions that reconcile helioseismology with thermal neutrino results.

Subject headings: cosmology: miscellaneous, dark matter, elementary particles, Sun: helioseismology

1. INTRODUCTION

The standard Λ CDM cosmological model has been successfully applied to explain the main characteristics of the Universe (see e.g. [Hinshaw et al. 2013](#); [Ade et al. 2013](#)). In particular, numerical simulations of collisionless cold Dark Matter (DM) describe the gravitational growth of infinitesimal primordial density perturbations, probed by the cosmic microwave background anisotropies, that lead to the formation of the present-day large-scale structure of the universe. These simulations provide us with a number of predictions about the structure of cold DM halos and their basic properties (see e.g. [Guo et al. 2013](#)). Although the standard cosmological model has proven to be highly successful in explaining the observed large-scale structure of the universe, it has been less successful on smaller scales. Recent data on low mass galaxies suggests that the inferred subhalo DM distributions have almost flat cores (see e.g. [de Blok 2010](#)), in contradiction with the cuspy profile distributions predicted by numerical simulations (see e.g. [Navarro et al. 2010](#)), and that sub halo numbers are overpredicted at both low mass and intermediate masses (see e.g. [Klypin et al. 1999](#)) and massive dwarf galaxy scales (see e.g. [Garrison-Kimmel et al. 2013](#)).

Some of the issues associated with dwarf galaxies can be addressed if the DM is more "collisional" (with

baryons) than currently considered in numerical simulations. This hypothesis favors constant-density cores with lower central densities than those coming from cold DM models, such as self interacting DM (see e.g., [Rocha et al. 2013](#)).

In addition, the closeness between Ω_{DM} and Ω_{b} , usually referred as cosmic coincidence, may suggest a profound link between the dark and the ordinary sectors. Indeed, although the two sectors have different macroscopic properties, the total amount of DM observed today could be produced in the early universe by a mechanism identical to baryogenesis, and therefore an asymmetry between DM particles and their antiparticles would be expected. A detailed account of current progress in asymmetric DM studies can be found in the literature (see e.g., [Petraki & Volkas 2013](#)).

All of these cosmological facts may suggest that dark and ordinary matter may have more properties in common than expected. In view of this, it is tantalizing to imagine that the dark world could be similarly complex (CP violating and asymmetric) and full of forces that are invisible to us (hidden parallel sector or mirror world⁸). The history of the early mirror universe has been studied in ref. ([Berezhiani et al. 2001](#)), while the impact of an hidden mirror sector in the CMB and LSS data can be found in ref. ([Berezhiani et al. 2005](#)). For a general review on the properties of a hidden world neighboring our own, see e.g. refs. ([Foot 2004b](#); [Berezhiani 2005](#)).

More specifically, since in our sector only long-range electromagnetic force and gravity affect the dynamical evolution of virialized astrophysical objects, the physics of a complex dark sector in which the matter fields are charged under an extra $U(1)$ gauge group is particularly interesting to study. Indeed, if the mass of the new gauge boson (dark photon) is smaller than the typical

⁸ The idea of a mirror world was suggested prior to the advent of the Standard Model (see e.g. Refs. ([Lee & Yang 1956](#); [Kobzarev et al. 1966](#))). The idea that the mirror particles might instead constitute the DM of the Universe was discussed in refs. ([Blinnikov & Khlopov 1982, 1983](#)).

¹ Centro Multidisciplinar de Astrofísica, Instituto Superior Técnico, Universidade Tecnica de Lisboa, Av. Rovisco Pais, 1049-001 Lisboa, Portugal

² Departamento de Física, Escola de Ciencia e Tecnologia, Universidade de Évora, Colégio Luis António Verney, 7002-554 Évora - Portugal

³ CP3-Origins and DIAS, University of Southern Denmark, Odense, Denmark

⁴ Institut d'Astrophysique, UMR 7095 CNRS, Université Pierre et Marie Curie, 98bis Blvd Arago, 75014 Paris, France

⁵ Department of Physics and Astronomy, The Johns Hopkins University, Baltimore, MD21218

⁶ Beecroft Institute for Cosmology and Particle Astrophysics, University of Oxford, Keble Road, Oxford OX1 3RH, UK

⁷ E-mails: (IL) ildio.lobes@tecnico.ulisboa.pt; (PP) panci@iap.fr; (JS) silk@astro.ox.ac.uk

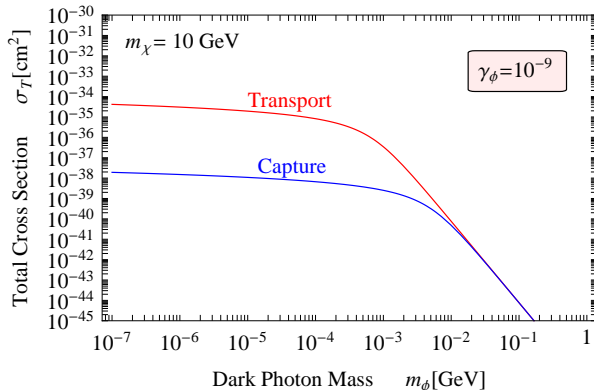


Figure 1. An illustrative example of the DM-hydrogen energy transfer cross section as a function of the mass of the dark photon m_ϕ for a fix value of the kinetic mixing parameter $\gamma_\phi = 10^{-9}$ and a DM mass $m_\chi = 10$ GeV. In blue is shown the scattering cross section responsible for the capture process σ_T^{cap} , while in red the one entering in the energy transport mechanism σ_T^{tra} computed at the present time ($T_c^0 = 1.57 \times 10^7$ K).

momenta exchanged in the scattering, the phenomenology of the dark world can in itself be as complicated as that of our sector (e.g. dark electromagnetism with quite large self-interactions), providing at the same time also a feeble long-range interaction between the two worlds (thanks to the kinetic mixing of the new $U(1)$ gauge boson with the photon). This implies in general that the dark world is more collisional than the standard cold DM, and therefore some of the previously mentioned problems can probably be solved (see e.g. [Loeb & Weiner 2011](#)).

In addition, since a long-range DM-nucleus interaction is enhanced for small momentum exchanges, this class of models can also relax the tension between the positive results of direct detection experiments (the annual modulation observed by DAMA ([Bernabei et al. 2008, 2010](#)) and CoGeNT ([Aalseth et al. 2011a,b](#)), and the hints of an observed excess of events on CRESST ([Angloher et al. 2012](#)) and CDMS-Si ([Agnese et al. 2013a,b](#))), and the constraints coming from null results (e.g. CDMS-Ge ([Ahmed et al. 2010](#)), XENON100 ([Aprile et al. 2011](#)) and very recently LUX ([Akerib et al. 2013](#))). The phenomenology of long-range DM-nucleus interactions in direct DM searches has been studied in Refs. ([Foot 2004a, 2008, 2010, 2012](#); [Fornengo et al. 2011](#); [Panci 2012](#)).

In this paper, we investigate how a DM-baryon Long Range Interaction (DMLRI), induced by the kinetic mixing of a new $U(1)$ gauge boson and the photon, affects the evolution of the Sun. The results obtained are then confronted with helioseismology data. The helioseismic data that we use was obtained by several international collaborations, such as the Solar and Heliospheric Observatory (SOHO) mission and the Birmingham Solar Oscillations Network (BiSON) observational network ([Turck-Chieze et al. 1997](#); [Basu et al. 2009](#)). Furthermore, we also discuss the constraints on the main parameters of long-range DM particle interactions which can be obtained from direct DM search data.

2. PROPERTIES OF DM WITH LONG-RANGE INTERACTIONS

In most of the classical models, one often assumes a symmetric dark sector in which the DM scattering off of

baryon nuclei is done by a contact-like interaction. In our study, we will instead focus on a class of asymmetric DM models in which the interaction between DM particles and target nuclei is mediated by a light messenger. If the typical momenta exchanged in the scattering is bigger than the mass of the mediator, a long-range interaction then arises.

A specific realization of this kind of picture is offered by particle physics models where a new $U(1)$ hidden gauge boson ϕ (dark photon) possesses a small kinetic mixing ϵ_ϕ with the photon. In this case, the interaction between a nucleus with mass m_T and electric charge Ze (Z is the number of protons in the baryon nucleus and e the electrical charge) and a DM particle with mass m_χ and dark charge $Z_\chi g_\chi$ (Z_χ and g_χ are the equivalent quantities of Z and e in the dark sector) is described in the non-relativistic limit by the following Yukawa potential (see e.g., [Fornengo et al. 2011](#)),

$$V(r) = \epsilon_\phi k_\chi \frac{Z\alpha}{r} e^{-m_\phi r}, \quad (1)$$

where $\alpha = e^2/4\pi$ is the electromagnetic fine structure constant and the parameter $k_\chi = Z_\chi g_\chi/e$ measures the strength of the DM-dark photon coupling. Here m_ϕ is the mass of the dark photon that acts like an electronic cloud which screens the charges of the particles involved in the scattering. Since both k_χ and ϵ_ϕ are unknown, we define $\gamma_\phi \equiv k_\chi \epsilon_\phi$ and we treat it as a free parameter of our model together with m_χ and m_ϕ . Before moving on we have however verify whether the symmetric component of χ in the dark sector is annihilated away or not. In general, since for this simple model the dominant annihilation channel is given by $\chi\chi \rightarrow \phi\phi$, we can put a lower bound on the parameter k_χ by demanding that the annihilation cross section into dark photons ($\langle\sigma v\rangle_{\phi\phi} = \pi\alpha^2 k_\chi^4/(2m_\chi^2)$) is bigger than the thermal one ($\langle\sigma v\rangle_{\phi\phi} \sim 1$ pb). In agreement with Refs. ([Tulin et al. 2013](#); [Kaplinghat et al. 2013](#)), this condition requires $k_\chi \geq k_\chi^\Omega = \bar{k}_\chi^\Omega \sqrt{m_\chi/\text{GeV}}$, where $\bar{k}_\chi^\Omega \simeq 7.5 \times 10^{-2}$. We shall come back to this point at the end of Sec. 3 because for this kind of models the DM-DM scattering can play an important role in the capture rate and in the energy transport by DM particles in the Sun.

The differential cross section, neglecting the form factor of the target nuclei⁹, can be simply obtained by performing the Fourier transform of Eq. 1 and it reads

$$\frac{d\sigma_T}{d\Omega} = \frac{\xi_\chi^2 \mu^2}{(q^2 + m_\phi^2)^2}, \quad (2)$$

where $\xi_\chi = 2\alpha Z \gamma_\phi$, $\mu = m_\chi m_T/(m_\chi + m_T)$ is the DM-nucleus reduced mass and $q = \sqrt{2m_T E_R}$ is the momenta exchanged in the interaction with E_R the recoil energy. As is apparent from the dependence on the dark photon mass, two different regimes clearly appear:

- ◇ *Point-like limit* ($q \ll m_\phi$): In this regime the interaction is of a contact type. Indeed the differential cross section turns out to be proportional to

⁹ The Sun being mostly composed of hydrogen and helium, we can justify neglecting the nuclear responses. On the other hand for the derivation of the direct detection constraints, we use the form factors provided in ref. ([Fitzpatrick et al. 2012](#)).

ξ_χ^2/m_ϕ^4 which plays the same role as Fermi’s constant in weak interactions. The interaction reduces to the “standard” spin-independent picture, apart from the fact that in this case, DM particles only couple with protons ($d\sigma_T/d\Omega \propto Z^2$).

- ◊ *Long-range limit* ($q \gg m_\phi$): In this regime, the differential cross section acquires an explicit dependence on the momenta exchanged in the interaction and therefore a Rutherford-like cross section arises ($d\sigma_T/d\Omega \propto 1/q^4$). This is extremely interesting because ideal experiments with very low energy threshold and light target nuclei (e.g. the Sun) are in principle more sensitive than the ones with high threshold and heavy targets (e.g. XENON100 and LUX). To give a concrete example, once DM particles are thermalized with baryons in the center of the Sun, their collisions occur with $q \simeq 1$ MeV considering a DM mass of 10 GeV. For direct detection experiments, the typical momenta transferred in the scattering is instead bigger ($q \gtrsim 20$ MeV). Thanks to this fact, we expect that DM models feature a long-range interaction with ordinary matter can affect the sound-speed radial profile of the Sun without being excluded by terrestrial experiments.

Having the differential cross section at our disposal, we assume that the normalization of both the capture rate and the transport of energy by DM particles in the Sun is controlled by the energy transfer cross section obtained by weighting Eq. (2) with $(1 - \cos\theta)$. This is of course a good estimator for the transport mechanism, while for the capture process the introduction of the same cross section is justified because the Sun’s escape velocity $v_{\text{esc}}(r)$ is much bigger than both the thermal velocity of baryons in the Sun and the typical dispersion velocity of the DM particles in the halo v_0 . In particular, we have checked that the error in the total rate is negligible, if we replace the total cross section in the rate per unit time $\Omega(w)$ given e.g. in Eq. 7 of (Kumar et al. 2012), with the energy transfer cross section computed for $w = v_{\text{esc}}(r)$. In the Born approximation¹⁰, the energy transfer cross section writes,

$$\sigma_T(v_{\text{rel}}) = \frac{2\pi\beta_\phi^2}{m_\phi^2} \left[\ln(1 + r_\phi^2) - \frac{r_\phi^2}{1 + r_\phi^2} \right], \quad (3)$$

where $\beta_\phi = \xi_\chi m_\phi / (2\mu v_{\text{rel}}^2)$, $r_\phi = 2\mu v_{\text{rel}} / m_\phi$, and v_{rel} is the relative velocity between the DM flux and the Sun. Unlike the customary DM models, in this case σ_T depends on v_{rel} in the long-range regime. Thanks to this main novelty, one therefore expects that the typical scattering cross section in the capture process differs compared to the one entering in the transport mechanism. On a more specific level, one has:

- ◊ *Capture*: In general, the infalling DM particles reach a given shell of radius r with a velocity $w(r) = \sqrt{u^2 + v_{\text{esc}}^2(r)}$, where u is the DM velocity at infinity with respect to the Sun’s rest frame.

¹⁰ The Born approximation is valid if $\beta_\phi \lesssim 0.1$ (see e.g. Loeb & Weiner (2011)). Since we are interested in the long-range regime ($\mu v_{\text{rel}}^2 \gg m_\phi$), it is easy to check that this approximation is very well satisfied.

Since both the thermal velocity of baryons in the Sun and the dispersion velocity of DM particles in the halo are much smaller than v_{esc} , we can assume as commented upon above that the relative velocity $v_{\text{rel}} \equiv w(r) \simeq v_{\text{esc}}(r)$. Furthermore, since the total number of DM particles captured by the Sun is independent on r , it is a good approximation to define an average infalling DM velocity by

$$\bar{w} = \frac{1}{M_\odot} \int_0^{R_\odot} d^3r w(r) \rho(r) \simeq 1120 \text{ km/s}. \quad (4)$$

Here $\rho(r)$ is the Sun’s mass density, $M_\odot = \int d^3r \rho(r) \simeq 1.98 \times 10^{30}$ kg is its total mass and $R_\odot \simeq 6.95 \times 10^{10}$ cm is its radius. As explained in more detail in the next section, the capture rate is then computed numerically considering a constant cross section $\sigma_T^{\text{cap}} = \sigma_T(\bar{w})$.

- ◊ *Transport*: In this case, the typical relative velocity for the scattering is much smaller than \bar{w} being due to DM particles thermalized together with the ordinary plasma in the center of the Sun. It is then a good approximation to assume $v_{\text{rel}} \equiv v_{\text{th}}$, where $v_{\text{th}} = \sqrt{2T_c/m_\chi}$ is the thermal speed and T_c is the time-dependent temperature in the Sun’s core. As explained in more detail in the next section, we compute the transport of energy numerically by considering $\sigma_T^{\text{tra}} = \sigma_T(v_{\text{th}})$. It is worth stressing that since the solar code follows the time evolution of the Sun, in the early stages the energy transport, and in turn the thermal conduction by DM particles, was much more efficient with T_c at that time being smaller than the present-day central temperature.

In this study, we focus on the interaction of DM with hydrogen – the most abundant chemical element in the Sun’s interior. Fig. 1 shows an illustrative example of the DM-hydrogen energy transfer cross section σ_T as a function of the mass of the dark photon m_ϕ for a fixed value of the kinetic mixing parameter $\gamma_\phi = 10^{-9}$ and a DM mass $m_\chi = 10$ GeV. On a more specific level we show in blue the scattering cross section responsible for the capture process σ_T^{cap} , while in red is shown the one entering into the energy transport mechanism σ_T^{tra} computed at the present time ($T_c^0 = 1.57 \times 10^7$ K). We can see that if the mass of the dark photon is smaller than a few MeV (long-range regime), the capture and the transport processes are controlled by different scattering cross sections. It is worth pointing out that in this limit, the ratio $\sigma_T^{\text{tra}}/\sigma_T^{\text{cap}}$ is barely dependent on m_ϕ , if m_χ is larger than the hydrogen mass. It instead depends on the mass of the DM particle through the thermal velocity relation and in particular for a 10 GeV candidate, $\sigma_T^{\text{tra}} \sim 10^3 \sigma_T^{\text{cap}}$. The main new aspect is actually given by this enhanced conduction in the inner part of the Sun compared to the usual DM models. Thanks indeed to this fact, DM particles, interacting via long-range forces with ordinary matter, can produce an impact on the helioseismology data without evading the constraints coming from direct DM search experiments.

In our analysis, we consider the observed sound speed radial profile of the Sun and compare it to the theoretical

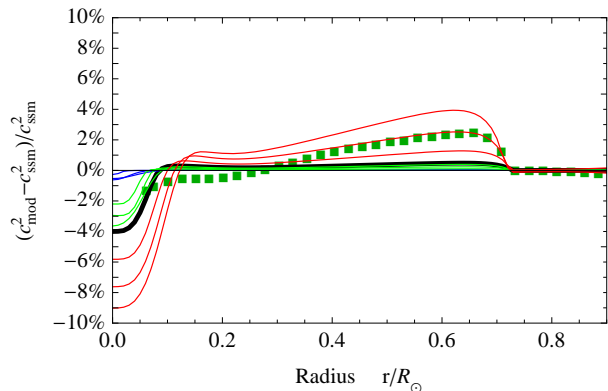


Figure 2. Comparison of sound speed differences: $\Delta c^2 = (c_{\text{mod}}^2 - c_{\text{ssm}}^2)/c_{\text{ssm}}^2$. c_{ssm}^2 is the sound speed of the SSM (e.g., Lopes & Turck-Chieze 2013) and c^2 is either c_{obs}^2 the observed sound speed (green-square dots: Turck-Chieze et al. 1997; Basu et al. 2009) or c_{mod}^2 the sound speed of a DMLRI solar model (continuous curves: $|\Delta c^2| < 2.0\%$ blue, $[2.0 \leq |\Delta c^2| \leq 4.0\%]$ green and $|\Delta c^2| > 4.0\%$ red). The DMLRI models were computed for the parameters (see text): $5 \text{ GeV} \leq m_\chi \leq 20 \text{ GeV}$; $0.1 \text{ keV} \leq m_\phi \leq 1 \text{ GeV}$ and $\gamma_\phi = 10^{-9}$. The black curve corresponds to a fiducial model with $m_\chi = 10 \text{ GeV}$ and $m_\phi = 10 \text{ keV}$. Note that the observational error in c_{obs} is multiplied by a factor 10.

prediction over a broad range of DM masses ($4 \text{ GeV} \leq m_\chi \leq 20 \text{ GeV}$), dark photon masses ($0.1 \text{ keV} \leq m_\phi \leq 1 \text{ GeV}$)¹¹ and kinetic mixing parameters ($10^{-12} \leq \gamma_\phi \leq 10^{-6}$). With these choices, the scattering cross-section spans a large interval of values from $5 \times 10^{-29} \text{ cm}^2$ to $8 \times 10^{-55} \text{ cm}^2$. The cross-section range of interest for the Sun corresponds to the values for which σ_T is close to the Sun’s characteristic scattering cross-section, $\sigma_\odot = m_p/M_\odot R_\odot^2$. From the zero-age mean-sequence (ZAMS) until the present age of the Sun (4.6 Gyear), σ_\odot takes values between $2.5 \times 10^{-32} \text{ cm}^2$ and $4 \times 10^{-36} \text{ cm}^2$.

3. DARK MATTER AND THE SUN

The Sun, as are all stars in the Milky Way, is immersed in a halo of DM. As with any other star in the galaxy, the Sun captures substantial numbers of DM particles during its evolution, but any impact on the star depends on the properties of these particles, as well as on the stellar dynamics and structure of the star. In general, for low-mass stars evolving in low density DM halos, the presence of DM inside the star changes its evolution by providing the star with a new mechanism to evacuate the heat produced in the stellar core (e.g., Lopes et al. 2002; Lopes & Silk 2002; Zentner & Hearin 2011; Lopes & Silk 2012a; Casanellas & Lopes 2013). This is quite different for stars evolving in DM halos of high density – as occurs during the formation of the first generation of stars. In these cases, the annihilation of DM particles supplies the star with an additional source of energy capable of substantially extending the lifetimes of these stars (Scott et al. 2009; Casanellas & Lopes 2009; Lopes et al. 2011; Scott et al. 2011).

The computation of the impact of DM in the evolution of the Sun is done by a modified version of the CESAM code (Morel 1997; Morel & Lebreton 2008),

¹¹ As we will see later, for masses below 0.1 keV the Sun’s sound speed profiles become independent on m_ϕ and therefore our results can also be extended for lighter mediators.

which has been widely used to compute the SSM and for modelling other stars by different research groups (Deheuvels et al. 2010; Turck-Chieze et al. 2010; Lopes 2013; Lopes & Turck-Chieze 2013). In this study, we follow a procedure identical to other studies published in the literature by some of us as well as other authors (e.g., Lopes et al. 2002; Lopes & Silk 2002; Cumberbatch et al. 2010; Taoso et al. 2010; Lopes & Silk 2010a,b; Hamerly & Kosovichev 2012; Lopes & Silk 2012a,b; Lopes et al. 2014). Nevertheless, there are some important differences between this study and the previous ones, which we will highlight in the remainder of this section.

As commented upon in the previous section, the impact of DM in the Sun’s interior depends on two major physical processes: the accumulation of DM inside the star, and the efficiency of DM in transferring energy from the core to the external layers. In any case, the density of DM in the halo is the single major ingredient affecting the impact of DM in the Sun. As usually done in these studies, we consider that the local density of DM is $\rho_\odot = 0.38 \text{ GeV/cm}^3$ (Gates et al. 1995, 1996; Catena & Ullio 2010; Salucci et al. 2010). The choice of this value is in part made to facilitate the comparison with other work. Still, this is a very reliable value: the most recent estimates of ρ_\odot made by two independent groups have obtained values of 0.3 GeV/cm^3 (Bovy & Tremaine 2012) and 0.85 GeV/cm^3 (Garbari et al. 2012). In particular (Garbari et al. 2012) argue that their new method is quite robust, and they have obtained their value at 90% confidence level. In our computation, we will also consider that the DM particles in the solar neighborhood have dispersion velocity $v_0 = 220 \text{ km/s}$ (see e.g., Bertone et al. 2005).

The accumulation of DM in the Sun’s core during its evolution from the beginning of the ZAMS until the present age (4.6 Gyear) is regulated by three physical processes: capture, annihilation and evaporation of DM particles. At each step of the evolution, the total number of DM particles N_χ , that is captured by the star is given by

$$\frac{dN_\chi(t)}{dt} = \Gamma_{\text{cap}} + \Gamma_\chi N_\chi(t) - \Gamma_{\text{ann}} N_\chi(t)^2 - \Gamma_{\text{eva}} N_\chi(t), \quad (5)$$

where Γ_{cap} , Γ_χ , Γ_{ann} and Γ_{eva} refer to the DM capture, self-capture, annihilation and evaporation rates respectively. It is worth noticing that, unlike previous studies, in this work we resolve numerically the equation (5) for each step of the star’s evolution. A detailed discussion about these processes can be found in the literature (e.g., Griest & Seckel 1987; Lopes et al. 2011).

The capture rate Γ_{cap} is computed numerically from the expression obtained by Gould (1987) as implemented by Gondolo et al. (2004). The scattering of DM particles with the baryons inside the Sun is the main factor affecting the capture rate Γ_{cap} . We restrict our study to the scattering of DM particles to the most abundant element, i.e., hydrogen. We consider that the capture rate is controlled by σ_T^{cap} obtained by substituting v_{rel} with the averaged infalling speed \bar{w} in Eq. (3) as briefly explained in the previous section. In particular, in the long-range regime ($r_\phi \gg 1$ or in terms of the exchanged

momenta, $q \gg m_\phi$), the DM-hydrogen energy transfer cross section responsible for the capture process is independent of m_χ and logarithmically dependent on m_ϕ . It reads

$$\lim_{r_\phi \gg 1} \sigma_T^{\text{cap}} = 4\pi \frac{\alpha^2 \gamma_\phi^2}{m_p^2 \bar{w}^4} L_\phi^{\text{cap}}(m_\phi) \simeq \left(\frac{\gamma_\phi}{10^{-9}}\right)^2 \left(\frac{L_\phi^{\text{cap}}}{\bar{L}_\phi^{\text{cap}}}\right) \cdot 1.1 \times 10^{-38} \text{ cm}^2, \quad (6)$$

where $L_\phi^{\text{cap}} = \ln(2m_p \bar{w}/m_\phi)$ is a sort of Coulomb logarithm that measures the strength of the screening effect in the capture process and $\bar{L}_\phi^{\text{cap}} \simeq 6.5$ is its value for $m_\phi = 10$ keV.

The other chemical elements are under-abundant, consequently their contribution for the capture of DM is negligible. The dependence of the scattering cross-section on the parameter space of long-range DM particles is given by equation (3). The description of how this capture process is implemented in our code is discussed in Lopes et al. (2011).

Since we assume a primordial asymmetry between particles and anti-particles in the dark sector, the annihilation rate Γ_{ann} is set to be zero. This condition, as we have briefly mentioned in Sec. 2 is justified if $k_\chi \geq k_\chi^\Omega \simeq \bar{k}_\chi^\Omega \sqrt{m_\chi/\text{GeV}}$.

The evaporation rate Γ_{eva} is relevant only for very light particles, i.e., particles with $m_\chi \leq 4$ GeV (Gould 1990). Kappl & Winkler (2011) estimated the evaporation mass for DM particles in the Sun, m_{eva} , to be such that $m_{\text{eva}} = 3.02 + 0.32 \log_{10}(\sigma_T/10^{-40} \text{ cm}^2)$ GeV. If $m_\chi \leq m_{\text{eva}}$ the DM particle escapes the solar gravitational field and consequently has no impact on the structure of the star. Kappl & Winkler (2011) also found that the evaporation of DM particles is completely irrelevant for $m \geq 8$ GeV. It is worth noticing the fact that because the evaporation boundary has an exponential dependency on the mass and the scattering cross-section of the DM particle (Gould 1990), it follows that if m_χ exceeds m_{eva} by a few percent, then the evaporation of DM particles is totally negligible. Furthermore it is also important to point out that our DM model can easily have a quite large self-interaction in the long-range regime with size similar to the electromagnetic scattering. If then this self-interaction is attractive (e.g. this can be obtained if the dark sector is composed by light and heavy species with a different sign of the dark charge $Z_\chi g_\chi$) we expect that Γ_{eva} can be set to zero for DM masses below 4 GeV as well, in such cases the properties of the dark plasma being similar to the ordinary one (electrons are indeed trapped in the Sun). We leave further discussion of this important effect for future studies.

In our computation, we use Γ_{eva} estimated by Busoni et al. (2013) in the regime where the Sun is optically thin with respect to the DM particles. Nevertheless, we restrict our analysis to particles with mass larger than 4 GeV, for which the evaporation rate is almost negligible.

Once gravitationally captured by the star, the DM particles thermalise with baryons after a few Kepler orbits

around the solar centre, colliding through elastic scattering with hydrogen and other elements, and thus providing the star with an alternative mechanism for the transport of energy. The relative efficiency of the DM energy transport in relation to the radiative heat transport depends on the Knudsen number, $K_\chi = l_\chi/r_\chi$ where l_χ is the free mean path of the DM particle inside the star and $r_\chi(m_\chi)$ is the characteristic radius of the DM distribution (Gilliland et al. 1986; Lopes et al. 2002) given by

$$r_\chi(m_\chi) = \left(\frac{3T_c}{2\pi G_N \rho_c m_\chi}\right)^{\frac{1}{2}} \simeq \left(\frac{10 \text{ GeV}}{m_\chi}\right)^{\frac{1}{2}} \left(\frac{T_c}{T_c^0}\right)^{\frac{1}{2}} \left(\frac{\rho_c}{\rho_c^0}\right)^{\frac{1}{2}} \cdot 0.035 R_\odot, \quad (7)$$

where $\rho_c^0 \simeq 8.3 \times 10^{25} \text{ GeV/cm}^3$ is the today's density of the Sun's core. Depending on the value of σ_T , the transport of energy by DM is local (conductive) or non-local, which corresponds to $K_\chi \ll 1$ or $K_\chi \gg 1$. In the conductive regime the effective luminosity carried by DM particles is proportional to $n_\chi l_\chi$, while in the non-local one to n_χ/l_χ . The maximal luminosity is instead achieved when $l_\chi \simeq 10 r_\chi$ (see e.g. Fig. 11 of Gould & Raffelt (1990)). Here n_χ is the number density of DM particles captured in the Sun which is given by $n_\chi(r) = n_0 \exp[-r^2/r_\chi^2]$ where $n_0 = N_\chi/(\pi^{3/2} r_\chi^3)$ (see e.g. Lopes et al. (2002)). We assume that the thermal conduction by DM particles is controlled by σ_T^{tra} obtained by substituting v_{rel} with the thermal speed v_{th} in Eq. (3) as briefly explained in the previous section. Unlike the cross section responsible for the capture process, in the long-range limit σ_T^{tra} depends on the DM mass via the thermal velocity v_{th} . It explicitly reads

$$\lim_{r_\phi \gg 1} \sigma_T^{\text{tra}} = \pi \frac{\alpha^2 \gamma_\phi^2 m_\chi^2}{m_p^2 T_c^2} L_\phi^{\text{tra}}(m_\chi, m_\phi, T_c) \simeq \left(\frac{m_\chi}{10 \text{ GeV}}\right)^2 \left(\frac{T_c}{T_c^0}\right)^2 \left(\frac{\gamma_\phi}{10^{-9}}\right)^2 \left(\frac{L_\phi^{\text{tra}}}{\bar{L}_\phi^{\text{tra}}}\right) \cdot 1.9 \times 10^{-35} \text{ cm}^2, \quad (8)$$

where $L_\phi^{\text{tra}}(m_\chi, m_\phi, T_c) = 1/2 \ln(8m_p^2 T_c/(m_\chi m_\phi^2))$ emulates the screening effect in the energy transport and $\bar{L}_\phi^{\text{tra}} \simeq 4.5$ is its value for $m_\phi = 10$ keV, $m_\chi = 10$ GeV and $T_c = T_c^0$. Once computed the energy transfer cross section the average mean free path in the long-range regime, can be estimated as

$$l_\chi = \left(\langle n_b \rangle \cdot \lim_{r_\phi \gg 1} \sigma_T^{\text{tra}}\right)^{-1} \simeq \left(\frac{10 \text{ GeV}}{m_\chi}\right)^2 \left(\frac{T_c^0}{T_c}\right)^2 \left(\frac{10^{-9}}{\gamma_\phi}\right)^2 \left(\frac{\bar{L}_\phi^{\text{tra}}}{L_\phi^{\text{tra}}}\right) \cdot 0.055 R_\odot, \quad (9)$$

where

$$\langle n_b \rangle = \frac{1}{R_\odot} \int_0^{R_\odot} dr n_b(r) \simeq 1.3 \times 10^{25} / \text{cm}^3, \quad (10)$$

is the average number density of baryons in the Sun and $n_b(r) \simeq \rho(r)/m_p$. Depending on the free parameters of the model scanned in our analysis, the

energy transfer cross section covers a broad range of values ($5 \times 10^{-29} \text{ cm}^2 \leq \sigma_T^{\text{tra}} \leq 8 \times 10^{-55} \text{ cm}^2$). In this case the corresponding range of the Knudsen number is ($5 \times 10^{-9} \leq K_\chi \leq 3 \times 10^{18}$). Both mechanisms of energy transport are considered in this study (Gilliland et al. 1986; Lopes et al. 2002). In the case of the non-local regime, we follow the numerical prescription of Gould & Raffelt (1990) rather than the original one proposed by Spergel & Press (1985).

We note that in the long-range limit, a Rutherford-like DM-baryon interaction can significantly enhance the energy transport ($\sigma_T^{\text{tra}} \gg \sigma_T^{\text{cap}}$) compared to the usual picture (for the standard spin-independent and spin-dependent cases, one always has $\sigma_T^{\text{tra}} = \sigma_T^{\text{cap}}$). Indeed, even if the capture cross section is around 10^{-39} cm^2 (this choice correspond to $\gamma_\phi = 3.3 \times 10^{-10}$), the DM particles can have a mean free path around $10 r_\chi$, providing then the maximum luminosity carried by DM particles. For the standard contact interaction and for the same cross section, the mean free path is much longer and therefore the luminosity is reduced being in this case the transport non-local. This is the main new element, and in particular, as we will see in Sec. 5, this class of models with enhanced energy transport can solve the so-called solar abundance problem without being excluded by direct searches experiments.

A similar conclusion can also be found in Ref. (Vincent & Scott 2013). In particular they implement the formalism of Gould & Raffelt (1990) in order to properly account for both velocity and exchanged momenta dependencies in the differential cross section. Although their method is more refined compare to the one we are using they did not incorporate their results in a solar simulation software yet.

The self-capture rate Γ_χ (as in Eq. 5) is neglected in our computation. Nonetheless, since in the long-range regime the self-interaction between the DM particles can be relatively large, we could expect a major impact in the Sun's evolution. As it will become clear later on we find that for $k_\chi \sim k_\chi^\Omega$ the contribution coming from Γ_χ is negligible because the two leading processes (capture and transport) compensate each other. On the other hand for larger value of the parameter k_χ we expect that the self-interaction entirely dominates the transport of energy in the Sun and therefore the results presented in this paper will be no longer valid. In the following, we estimate the impact of including the self-capture in Equation (5).

The starting point is the definition of the self-capture energy transfer cross section σ_χ^{cap} that in the Born approximation can be computed by substituting in Eq. 3, $\mu \rightarrow m_\chi/2$ and $\gamma_\phi \rightarrow k_\chi$. Since the DM particles occupy a very small range of radii within the Sun, it reads

$$\lim_{r_\phi \gg 1} \sigma_\chi^{\text{cap}} = 16\pi \frac{\alpha^2 k_\chi^2}{m_\chi^2 w(0)^4} L_{\chi\phi}^{\text{cap}}(m_\phi) \simeq \left(\frac{10 \text{ GeV}}{m_\chi}\right)^2 \left(\frac{k_\chi}{k_\chi^\Omega}\right)^2 \left(\frac{L_{\chi\phi}^{\text{cap}}}{L_{\chi\phi}^{\text{cap}}}\right) \cdot 9.6 \times 10^{-25} \text{ cm}^2, \quad (11)$$

where $w(0) \simeq 1400 \text{ km/s}$ is the infalling velocity of the DM particles at $r = 0$. Here $L_{\chi\phi}^{\text{cap}} = \ln(m_\chi w(0)/m_\phi)$ is the Coulomb logarithm for the self-capture process and

$\bar{L}_{\chi\phi}^{\text{cap}} \simeq 8.4$ is its value for $m_\phi = 10 \text{ keV}$. Since the self-capture cross section, in the long-range regime is very big, we have also to consider the capture of DM particles in the halo by other DM particles that have already been captured within the Sun. This effect can lead to exponential growth in the number of captured dark matter particles as a function of time until the number of particles captured has become so large that the star is optically thick to DM. As pointed out by Taoso et al. (2010), the number of DM particles captured, including the self-interactions, is then given by

$$\begin{cases} N_\chi^{\text{w}}(t) = \frac{\Gamma_{\text{cap}}}{\Gamma_\chi} (e^{\Gamma_\chi t} - 1) & \text{for } t \leq \hat{t}, \\ N_\chi^{\text{w}}(t) = \left(\Gamma_{\text{cap}} + \hat{\Gamma}_\chi\right) (t - \hat{t}) + N_\chi^{\text{w}}(\hat{t}) & \text{for } t > \hat{t}, \end{cases} \quad (12)$$

where \hat{t} is the time at which the Sun becomes optically thick to DM, $N_\chi^{\text{w}}(\hat{t}) = \pi r_\chi^2(m_\chi)/\sigma_\chi^{\text{cap}}$ is the critical number of DM particles captured due to the self-interaction and $\hat{\Gamma}_\chi = \Gamma_\chi N_\chi^{\text{w}}(\hat{t}) \simeq (10 \text{ GeV}/m_\chi)^2 \cdot 5.5 \times 10^{26} \text{ s}^{-1}$ is the critical rate. In Eq. (12) the capture and self-capture rates, in the long-range regime, can be estimated by the following analytic equations:

$$\Gamma_{\text{cap}} = \sqrt{\frac{3}{2}} \frac{\rho_\chi}{m_\chi} \lim_{r_\phi \gg 1} \sigma_T^{\text{cap}} \frac{v_{\text{esc}}^2(R_\odot)}{v_0} N_\odot \langle \phi \rangle \frac{\text{erf}(\eta)}{\eta} \simeq \left(\frac{10 \text{ GeV}}{m_\chi}\right) \left(\frac{\gamma_\phi}{10^{-9}}\right)^2 \left(\frac{L_\phi^{\text{cap}}}{L_\phi^{\text{cap}}}\right) \cdot 2.5 \times 10^{26} \text{ s}^{-1}, \quad (13)$$

and

$$\Gamma_\chi = \sqrt{\frac{3}{2}} \frac{\rho_\chi}{m_\chi} \lim_{r_\phi \gg 1} \sigma_\chi^{\text{cap}} \frac{v_{\text{esc}}^2(R_\odot)}{v_0} \langle \phi_\chi \rangle \frac{\text{erf}(\eta)}{\eta} \simeq \left(\frac{10 \text{ GeV}}{m_\chi}\right)^3 \left(\frac{k_\chi}{k_\chi^\Omega}\right)^2 \left(\frac{L_{\chi\phi}^{\text{cap}}}{L_{\chi\phi}^{\text{cap}}}\right) \cdot 2.9 \times 10^{-17} \text{ s}^{-1}. \quad (14)$$

with $\langle \phi \rangle \simeq 3.29$, $\langle \phi_\chi \rangle \simeq 5.13$ and $\eta \simeq 1.29$ (see e.g. Zentner (2009)). The critical time \hat{t} can then be obtained from the first line of Eq. (12) by substituting t with \hat{t} and it reads explicitly

$$\hat{t} = \frac{1}{\Gamma_\chi} \ln(1 + \Delta_N) \simeq 0.24 t_\odot \cdot \left(\frac{m_\chi}{10 \text{ GeV}}\right)^3 \left(\frac{\bar{k}_\chi^\Omega}{k_\chi}\right)^2 \left(\frac{\bar{L}_{\chi\phi}^{\text{cap}}}{L_{\chi\phi}^{\text{cap}}}\right) \ln(1 + \Delta_N), \quad (15)$$

where $\Delta_N = \hat{\Gamma}_\chi/\Gamma_{\text{cap}}$ and $t_\odot \simeq 4.567 \times 10^9$ years.

Imposing now the constraint $k_\chi \gtrsim \bar{k}_\chi^\Omega \sqrt{m_\chi/\text{GeV}}$ in order that the symmetric component of χ is depleted in the early universe, one can check from the equations above that $\hat{t} \ll t_\odot$ for most of the parameter space considered in our analysis. In this case we can easily estimate which is the present time ratio between the number of DM particles captured including the self-interaction (the second line of Eq. 12) and those captured neglecting this important effect (the analytic standard solution without the

self interaction is $N_\chi(t_\odot) = \Gamma_{\text{cap}} t_\odot$). It reads

$$\frac{N_\chi^w(t_\odot)}{N_\chi(t_\odot)} \simeq 1 + \Delta_N, \quad (16)$$

where the function Δ_N has been defined in Eq. (15) and writes explicitly

$$\Delta_N = \frac{r_\chi^2(m_\chi) m_p^2 \bar{w}^4}{4N_\odot \alpha^2 \gamma_\phi^2 L_\phi^{\text{cap}}(m_\phi)} \frac{\langle \phi_\chi \rangle}{\langle \phi \rangle} \simeq 2.2 \cdot \left(\frac{10 \text{ GeV}}{m_\chi} \right) \left(\frac{10^{-9}}{\gamma_\phi} \right)^2 \left(\frac{\bar{L}_\phi^{\text{cap}}}{L_\phi^{\text{cap}}} \right). \quad (17)$$

As is apparent, since the luminosity carried by the DM particles is proportional to the number density of them, the increase in the number of DM particles captured due to the self-interaction described in Eq. (16) would go in the direction of increasing the effects pointed out in this paper.

However, there is a countervailing effect associated with quite large DM self interaction. Indeed, when the Sun becomes optically thick to its own DM the mean free path become in general shorter. Therefore the luminosity carried by DM particles in the conductive regime ($K_\chi \ll 1$) is reduced and in turn the effects pointed out in this paper will then decrease. In order now to quantify this effect, the first thing that one has to define is of course the average mean free path of the DM particles in the Sun. Assuming now a Maxwell-Boltzmann distribution for the DM particles such that $n_\chi^w(r) = n_0^w \exp[-r^2/r_\chi^2]$ where $n_0^w = N_\chi^w/(\pi^{3/2} r_\chi^3)$, it writes

$$l_\chi^w = l_\chi \left(1 + l_\chi \langle n_\chi \rangle \cdot \lim_{r_\phi \gg 1} \sigma_\chi^{\text{cap}} \right)^{-1}, \quad (18)$$

where

$$\langle n_\chi \rangle = \frac{1}{R_\odot} \int_0^{R_\odot} dr n_\chi(r) = \frac{N_\chi^w}{2\pi} \frac{\text{erf}(R_\odot/r_\chi)}{R_\odot r_\chi^2}, \quad (19)$$

is the average number density of DM particles in the Sun. In analogy with Eq. (16), we can then estimate which is the present time ratio between the average mean free path including the self-interaction (Eq. (18)) and the one neglecting this important effect (the mean free path without the self-interaction l_χ is given in Eq. (9)). By means now of the second line of Eq. (12), the total number of DM captured due to the self-interaction can be written as $(1 + \Delta_N)\Gamma_{\text{cap}} t_\odot$ and therefore

$$\frac{l_\chi^w}{l_\chi} = (1 + (1 + \Delta_N) \Delta_l)^{-1}, \quad (20)$$

where the function Δ_l is given by

$$\Delta_l = \frac{\Gamma_{\text{cap}} t_\odot}{2\pi} \frac{\text{erf}(R_\odot/r_\chi)}{R_\odot r_\chi^2} \lim_{r_\phi \gg 1} \frac{\sigma_\chi^{\text{cap}}}{\sigma_T^{\text{tra}}} \simeq 0.054 \cdot \left(\frac{10 \text{ GeV}}{m_\chi} \right)^4 \left(\frac{k_\chi}{k_\chi^\Omega} \right)^2 \left(\frac{L_l}{\bar{L}_l} \right). \quad (21)$$

Here $L_l = L_{\chi\phi}^{\text{cap}} L_\phi^{\text{cap}} / L_\phi^{\text{tra}}$ and $\bar{L}_l \simeq 12$ is its value for $m_\chi = 10 \text{ GeV}$ and $m_\phi = 10 \text{ keV}$. It is worth noticing that

the transport is mainly conductive once the constraint $k_\chi \gtrsim \bar{k}_\chi^\Omega \sqrt{m_\chi/\text{GeV}}$ is imposed.

Having now Eqs. (16,20) at our disposal, we can finally estimate the effect of the self-interaction on the Sun's sound speed profiles. Indeed since the Sun's sound speed profiles are related with the effective luminosity carried by DM particles, in the conductive regime the ratio $\mathcal{Y}_{\text{SI}} \equiv n_\chi^w l_\chi^w / n_\chi l_\chi$ is a good estimator which can be used to quantify the effect of the self-interaction in our results presented in the next section. It can be written in a compact form as

$$\mathcal{Y}_{\text{SI}} = \left(\frac{1}{1 + \Delta_N} + \Delta_l \right)^{-1}. \quad (22)$$

Considering now a fiducial model with $m_\chi = 10 \text{ GeV}$, $m_\phi = 10 \text{ keV}$ and $\gamma_\phi = 10^{-9}$ we have found that $1.17 \gtrsim \mathcal{Y}_{\text{SI}} \gtrsim 1$ for $k_\chi^\Omega \gtrsim k_\chi \gtrsim 1.13 k_\chi^\Omega$. The reason of that relies on the fact that there is a compensation in the Sun's sound speeds profiles between the larger number of the DM captured due to the self-interaction and the shorter mean free path. The range of the parameter k_χ in which $\mathcal{Y}_{\text{SI}} \sim 1$ does not depends too much on γ_ϕ and m_ϕ , while it scales as m_χ^{-3} with the DM mass.

On the other hand, if $k_\chi \gtrsim 1.5 k_\Omega$, the ratio $\mathcal{Y}_{\text{SI}} \simeq 1/\Delta_l$. In that case there is not an efficient compensation and therefore \mathcal{Y}_{SI} can reach even small value¹². In view of these facts we can conclude that is a good approximation neglecting the self-capture rate in Eq. (5) if $k_\chi \sim k_\chi^\Omega$. Thanks to this constraint we can fix $k_\chi = k_\chi^\Omega$ and directly present the final results in terms of the kinetic mixing parameter $\epsilon_\phi = \gamma_\phi/k_\chi^\Omega$.

4. DISCUSSION

The impact of DM in the Sun is studied by inferring the modifications that DM causes to the Sun's structure and to the solar observables. In the following, the standard solar model (SSM; e.g., [Turck-Chieze & Lopes 1993](#); [Lopes 2013](#)) is used as our model of reference, which predicts solar neutrino fluxes and helioseismology data consistent with current measurements. The excellent agreement obtained between theory and observation results from the combined effort between the fields of helioseismology and solar modelling, a collaboration extended by several decades which lead to a high precision description of physical processes present inside the Sun ([Turck-Chieze & Couvidat 2011](#); [Turck-Chieze & Lopes 2012](#)). This was very relevant in the case of the physical processes related with microscopic physics, including the equation of state, opacities, nuclear reactions rates, and microscopic diffusion of helium and heavy elements. A detailed discussion about current predictions of the SSM and their uncertainties can be found in the literature (e.g., [Turck-Chieze & Lopes 1993](#); [Serenelli et al. 2009](#); [Guzik & Mussack 2010](#); [Turck-Chieze et al. 2010](#); [Lopes & Turck-Chieze 2013](#); [Lopes 2013](#); [Lopes & Silk 2013](#)).

¹² For example, considering the maximal value of $k_\chi = 1/\sqrt{\alpha} \simeq 11.7$ allowed by perturbation theory, we get $\mathcal{Y}_{\text{SI}} \simeq 7.5 \times 10^{-4}$ for the benchmark model.

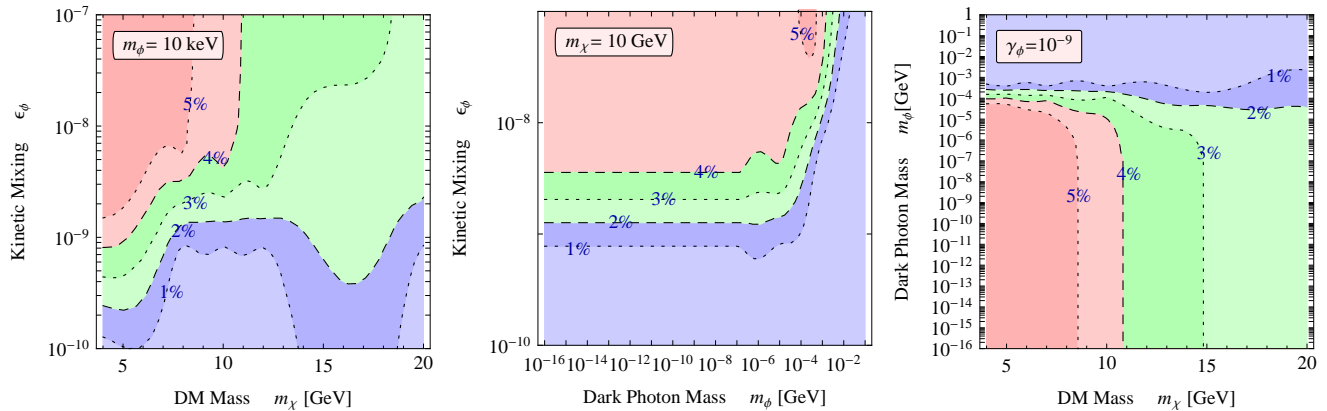


Figure 3. The maximum sound speed difference $\Delta c_{\max}^2 = \max[(c_{\text{mod}}^2 - c_{\text{ssm}}^2)/c_{\text{ssm}}^2]$ in the full parameter space of DMLRI models $(\epsilon_\phi, m_\chi, m_\phi)$ once the constraint $k_\chi = k_\chi^\Omega(m_\chi)$ is imposed. *Left panel:* Parameter space projected in the (m_χ, ϵ_ϕ) plane keeping fix $m_\phi = 10$ keV; *Central panel:* Parameter space in the (m_ϕ, ϵ_ϕ) plane considering $m_\chi = 10$ GeV; *Right panel:* Projection of the parameter space in the (m_χ, m_ϕ) plane for a fix $\gamma_\phi = \epsilon_\phi k_\chi^\Omega(m_\chi) = 10^{-9}$. In all panels the red(blue) areas individuate the regions of the parameter space where $\Delta c_{\max}^2 > 4\%$ ($\Delta c_{\max}^2 < 2\%$) while those in light green refer to the regions where the agreement with helioseismic data is better than the SSM ($2\% < \Delta c_{\max}^2 < 4\%$). All the DMLRI models in the red regions are excluded since they produce a large impact on the Sun's core sound speed profile. The DM halo in the Galaxy has been assumed in the form of an isothermal sphere with local energy density $\rho_\odot = 0.38$ GeV/cm³ and velocity dispersion $v_0 = 220$ km/s.

In Fig. 2 we compare the sound speed profile of SSM with the sound speed computed by an inversion technique from helioseismology data (Turck-Chieze et al. 1997; Basu et al. 2009). The green square dots correspond to the relative sound speed difference $\Delta c_{\text{obs}} = (c_{\text{obs}}^2 - c_{\text{ssm}}^2)/c_{\text{ssm}}^2$, where c_{ssm} and c_{obs} are the sound speed from SSM and helioseismic data. Δc_{obs} is smaller than 2% throughout the solar interior, above 20% and below 90% of the Sun's radius. Although agreement between c_{ssm} and c_{obs} is very good, a discrepancy remains between the present SSM and helioseismic data, from which there is no obvious solution Turck-Chieze & Couvidat (2011). It is worth noticing that the quality of the sound speed inversion is highly reliable, as most of the helioseismic data has a relative precision of measurements larger than 10^{-4} . Contrarily, in the Sun's inner core below $0.2 R_\odot$, the seismology data available is quite sparse and consequently the sound speed inversion is less reliable (cf. Fig. 2). As pointed out by Turck-Chieze & Couvidat (2011) the inversion of the sound speed profile in the Sun's inner core is limited by the low number acoustic frequencies measured (see Table 1 in Turck-Chieze & Lopes (2012) and references therein), as well as by the weak sensitivity of the eigenfunctions of global acoustic modes to the structure of the Sun's core. This difficulty can only be overcome with the positive detection of gravity modes. Equally, in the most external layers of the Sun, the inversion of the sound speed profile is not possible, mainly due to the fact that the inversion technique breaks down (acoustic oscillations are no-longer adiabatic), as a complex interaction occurs between convection, magnetic fields and acoustic oscillations (Gough 2012; Lopes & Gough 2001).

Accordingly, for the purpose of this study, we choose to consider the theory-observation uncertainty to be of the order of 4% rather than 2%. In the remainder of the article we will refer to this value as the *SSM uncertainty*, meaning the undistinguished uncertainty related to the physical processes of the SSM or helioseismology sound speed inversion.

The DMLRI solar models were obtained in an identical manner to the SSM, by adjusting the initial helium Y_i and the mixing length parameter α_{MLT} in such a way that at the present age (4.6 Gyear), these solar models reproduced the observed values of the mass, radius and luminosity of the Sun, as well as the observed photospheric abundance ratio $(Z/X)_\odot$, where X and Z are the mass fraction of hydrogen and the mass fraction of elements heavier than helium, respectively. Fig. 2 shows a comparison between SSM and different DMLRI models. The different continuous lines correspond to the squared sound speed difference $\Delta c_{\text{mod}}^2 = (c_{\text{mod}}^2 - c_{\text{ssm}}^2)/c_{\text{ssm}}^2$ where c_{mod} is the sound speed of DMLRI solar models. These models are obtained for a fiducial value of $\gamma_\phi = 10^{-9}$ and different values of m_χ and m_ϕ . The most important point about Fig. 2 is the fact that there are some DMLRI solar models that can resolve the current discrepancy with helioseismology data, as Δc_{mod}^2 reproduces the observed discrepancy Δc_{obs}^2 .

In DMLRI models, the DM impact is most visible in the core of the star where the DM particles accumulate. However, because the solar models are required to have the current observed values of radius and luminosity, a decrease of the production of nuclear energy in the Sun's core due to the reduction of the central temperature (caused by the thermalisation of DM with baryons), is compensated by an increase of the sound speed in the radiative region. In Fig. 2 we show an illustrative DMGRI solar model with benchmark parameters: $m_\chi = 10$ GeV, $m_\phi = 10$ keV and $\gamma_\phi = 10^{-9}$ (black curve). Moreover, all the DMLRI solar models have an identical impact behaviour on the solar structure, however, based upon the parameters m_χ and m_ϕ it is possible to distinguish three sets of models: *i*) DMLRI models for which the squared sound speed difference is larger than the *SSM uncertainty* (red curves); *ii*) DMLRI models for which the agreement with the helioseismic data is better than the current SSM (green curves); *iii*) DMLRI models for which the squared sound speed difference is smaller than the *SSM uncertainty* (blue curves). Although, there is a large set of

DMLRI models (*red* and *green curves*) for which Δc_{mod}^2 tends to agree Δc_{obs}^2 , as for those models for which the central value of c_{mod}^2 varies more than 4%, the central temperature will change for an identical amount. Consequently, the solar neutrino fluxes of these models become strongly in disagreement with the current neutrino flux observations (e.g., [Lopes & Silk 2012b,a](#)). Therefore, we make the conservative option in this preliminary study to only consider models for which the central temperature does not change very much from the SSM (*green curves* DMLRI models).

Fig. 3 shows the maximum sound speed difference $\Delta c_{\text{max}}^2 = \max[(c_{\text{mod}}^2 - c_{\text{ssm}}^2)/c_{\text{ssm}}^2]$ in the full parameter space of DMLRI models $(\epsilon_\phi, m_\chi, m_\phi)$ once the constraint $k_\chi = k_\chi^\Omega(m_\chi)$ is imposed. The represented percentages are performed for $r \leq 0.3 R_\odot$. On a more specific level in the right panel of Fig. 3 we project the parameter space in the (m_χ, ϵ_ϕ) plane by choosing $m_\phi = 10$ keV. In the central plane the (m_ϕ, ϵ_ϕ) plane is shown for $m_\chi = 10$ GeV, while on the left panel, the parameter space is projected in the (m_χ, m_ϕ) plane keeping fix $\gamma_\phi = \epsilon_\phi k_\chi^\Omega(m_\chi) = 10^{-9}$. Once Δc_{max}^2 is larger than the SSM uncertainty it is reasonable to exclude all DMLRI models, since they produce a large impact on the Sun's core sound speed profile (*red regions*). On the other hand, if Δc_{max}^2 is in the range 2% – 4% the agreement with the helioseismic data, as commented upon above, is improved (*green regions*). For instance, we find that DM particles with a mass in the range 4 GeV–8.5 GeV coupled with ordinary baryons via a kinetic mixing parameter ϵ_ϕ bigger than 5×10^{-9} , produce a very large impact on the Sun's core in the long-range regime (m_ϕ smaller than a few MeV). Therefore they can be excluded as possible DM candidates. On the other hand, we can see that DM particles with a mass of the order of 10 GeV, a kinetic mixing parameter $\sim 10^{-9}$ and a mediator with a mass smaller than a few MeV improve the agreement between the best solar model and the helioseismic data. This is quite interesting since direct DM searches experiments, as we shall see in the next section, either do not, or barely exclude, these kinds of DM models with long-range interactions with baryons. Furthermore, it is worth noticing that for very light dark photon (m_ϕ smaller than few keV), and for $\epsilon_\phi \gtrsim 3.33 \times 10^{-9}/k_\chi^\Omega(m_\chi)$ the transport occurs in the conductive regime. In this case, as we can see in the figure, our results are independent on m_ϕ , because the effective luminosity carried by DM particles in the conductive regime is proportional to $n_\chi l_\chi \propto \sigma_T^{\text{cap}}/\sigma_T^{\text{tra}}$. This is important because, as we will see in the next section, the complementary constraints coming from supernova observations and astrophysical or cosmological arguments are very weak for very light mediators.

5. COMPLEMENTARY CONSTRAINTS

In this section, we present the complementary constraints which are relevant for DMLRI models. A first class of them come from terrestrial direct detection experiments. In particular, since the interactions considered in our work is spin-independent, we only compute the constraints coming from the XENON100 and LUX experiments. The statistical analysis used to treat the datasets can be found in ([Cirelli et al. 2013](#)) where

the authors have provided a complete sets of numerical tools for deriving the bounds in direct searches in a completely model independent way. Without entering in the details of this work we can compute the bounds in the relevant parameter space of our model following the main steps summarized in Sec. 6 of ([Cirelli et al. 2013](#)). In particular, as pointed out in the first three steps (1a-1c), we have to identify the non-relativistic operator and its coefficient associated with a Yukawa-type interaction given in Eq. (1). Since this interaction is spin independent the operator is simply the identity, while the non-relativistic coefficient is given by $c_Y^p = 16\pi\alpha\gamma_\phi m_p m_\chi/(q^2 + m_\phi^2)$ (see e.g. ([Panci 2014](#)) for details). Thanks now to ready-made scaling functions provided in the webpage of ([Cirelli et al. 2013](#)), the bounds on the parameter space of our model can be obtained by following the last two steps (2a-2b). In Fig. 4 we show the constraints in the relevant parameter spaces of our model. As we did in the previous section, we project the parameter space in the (m_χ, ϵ_ϕ) plane (left panel), (m_ϕ, ϵ_ϕ) plane (central panel) and (m_χ, m_ϕ) plane (right panel). The dark blue (red) lines refer to the constraints coming from XENON100(LUX), while the different hatching (dotted, dashed-dotted, dashed) indicates the three values of the third direction in the parameter space that we kept fixed ($m_\phi = (1, 0.1, \leq 0.01)$ GeV on the left panel, $m_\chi = (6, 10, 14)$ GeV on the central panel and $\gamma_\phi = \epsilon_\phi k_\chi^\Omega(m_\chi) = (10^{-8}, 10^{-9}, 10^{-9.5})$ on the right panel). The areas of the parameter space above the first and second plots, and the ones below the third plot are excluded. Similar constraints can also be found in Ref. ([Kaplinghat et al. 2013](#)). We can see that in the long-range regime (mediator masses below roughly 10 MeV), the constraints becomes independent of m_ϕ . Indeed in this case, the interaction is Rutherford-like and therefore the differential cross section in Eq. (2), which sets the normalization of the total number of events in certain experiments, solely depends on the exchanged momentum q . By virtue of this fact, we can just use the left plot of Fig. 4 and compare it directly with the results shown in Fig. 3. We can see that in the relevant DM mass range that affects helioseismic data (4–20) GeV, the constraints, coming from the LUX experiments, exclude DMLRI models that are coupled with baryons through kinetic mixing parameters larger than roughly ($\gtrsim 10^{-7}, 5 \times 10^{-10}$). Therefore, as is apparent, long-range spin-independent DM-baryon interactions can easily improve the agreement between the best solar model and the helioseismic data without being excluded by direct detection experiments for DM masses in the range (4-12) GeV. Indeed, as we have already pointed out, the Sun is an ideal experiments for DM models which posses an enhanced cross section with baryons for small momentum exchanges.

A second class of complementary constraints that only depends on the properties of the dark photon (kinetic mixing parameter ϵ_ϕ and its mass m_ϕ) are those coming from supernovæ observations and beam dump neutrino experiments. These are presented, for instance, in the (m_ϕ, ϵ_ϕ) plane in Fig. 6 ($m_\phi > 10^{-3}$ GeV) and Fig. 7 ($m_\phi < 10^{-3}$ GeV) of ([Essig et al. 2013](#)). We can see that the most stringent constraints are the ones coming from

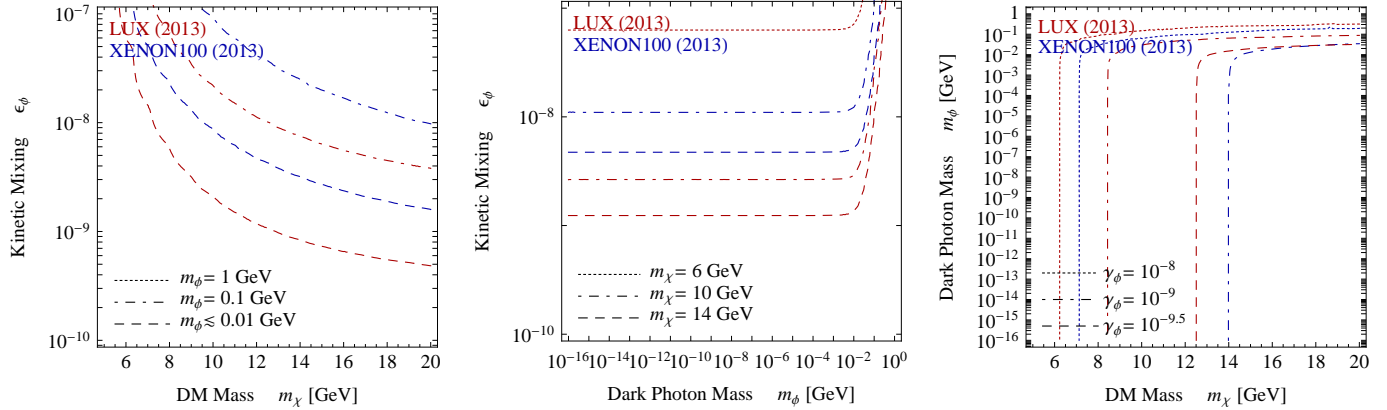


Figure 4. Direct detection constraints in the relevant parameter space of DMLRI models once the constraint $k_\chi = k_\chi^\Omega(m_\chi)$ is imposed. *Left panel:* Parameter space projected in the (m_χ, ϵ_ϕ) plane; *Central panel:* Parameter space in the (m_ϕ, ϵ_ϕ) plane; *Right panel:* Projection of the parameter space in the (m_χ, m_ϕ) plane. In all panels, the dark blue (red) lines refer to the constraints coming from XENON100 (LUX), while the different hatching (dotted, dashed-dotted, dashed) indicates the three values of the third direction in the parameter space we kept fixed ($m_\phi = (1, 0.1, \leq 0.01)$ GeV on the left panel, $m_\chi = (6, 10, 14)$ GeV on the central panel and $\gamma_\phi = \epsilon_\phi k_\chi^\Omega(m_\chi) = (10^{-8}, 10^{-9}, 10^{-9.5})$ on the right panel). Like in Fig. 3, the bounds are computed by assuming an isothermal halo with $\rho_\odot = 0.38$ GeV/cm³ and $v_0 = 220$ km/s.

supernova observations (namely the energy loss observed from SN1987a) and from astrophysical, or cosmological arguments: they indeed constrain relatively small kinetic mixing parameters (ϵ_ϕ above roughly $(10^{-11} - 10^{-10})$) and dark photon masses in the range ($10^{-9} \lesssim m_\phi \lesssim 0.2$) GeV. Therefore they ruled out all the parameter space above $m_\phi \gtrsim 10^{-9}$ GeV shown in the central panel of Fig. 3. On the other hand for very light messengers, they become extremely weak ($\epsilon_\phi \gtrsim 10^{-8}$) being the direct production of dark photons forbidden by kinematical reasons. In that case all the parameter space will be then reopened since, as we commented upon in the last paragraph of Sec. 4, the amplitude of the Sun’s sounds speed profiles is independent on m_ϕ (see e.g. the central panel of Fig. 3).

A third class of constraints which instead solely depend on the characteristics on the dark sector itself are those coming from self-interactions. Indeed, since for this type of model, the DM-DM scattering is not suppressed by ϵ_ϕ , the self-interactions, especially in the long-range limit, can easily reach large values, affecting the dynamics of virialized astrophysical objects. In Refs. (Tulin et al. 2013; Kaplinghat et al. 2013), the constraints on m_ϕ coming from the observations of a few elliptical DM halos have been presented. These constraints are in general very stringent for DM masses below 10 GeV: in this case, in fact, the time over which energy is transferred in the system is extremely rapid and therefore a spherical DM halo tends to form in contradiction with observations. In particular, dark photon masses below roughly 100 MeV are excluded. However, the derivation of this last class of constraints is very uncertain, both from the theoretical and experimental side, because we do not really know how virialized astrophysical objects are formed in the presence of a DM sector with long-range interactions. Indeed, since the self-interaction needed to change their dynamics is in general of the order of the Thompson scattering ($\sigma_{\text{em}} \simeq 10^{-24}$ cm²), from trivial dimensional analysis of such large cross sections, the following rough estimate yields that the self-interaction is of a long-range type in most of the virialized astrophysical objects under

the assumption that the DM-dark photon coupling is of the order of α . In this case, the probability to radiate a dark photon in the scattering process is different from zero and therefore it might well be possible that the DM sector is dissipative just like our sector. The time over which energy is transferred in the system is no longer a good indicator, since the relevant quantity that describes the dynamical evolution of the system is now the cooling time: in particular, for a DM sector composed of heavy and light species, the dissipation time due to the soft emission of dark photons (dark bremsstrahlung) can be smaller than the age of the virialized astrophysical objects (see e.g. Fan et al. 2013a,b; McCullough & Randall 2013). In this case, the system is no longer stable and in general it starts to collapse. By virtue of this fact, we do not consider this last class of constraints, since a more dedicated and careful analysis also involving numerical simulations is clearly needed.

6. CONCLUSION AND SUMMARY

We have examined how DM-baryon long-range interactions can affect the Sun’s sound speed radial profile. The phenomenological approach used in our analysis lets us explore all the parameter space from the contact regime to the long-range regime. We find that DM particles lighter than 8.5 GeV coupled with ordinary baryons through a kinetic mixing parameter γ_ϕ bigger than 5×10^{-9} , produce a very large impact on the Sun’s core in the long-range regime (m_ϕ smaller than few MeV). Therefore they can be excluded as possible DM candidates. However, solar models for which the DM particle has a mass of 10 GeV and the mediator a mass smaller than 1 MeV improve the agreement with helioseismic data. Nevertheless, when the mass of the dark photon is larger than 10 MeV the impact on the Sun’s structure is very small, being in this case the interaction of a contact-type (standard spin-independent picture). In particular, the results obtained here reveal that DM models featuring a long-range interaction with ordinary matter can affect the sound-speed radial profile and in turn probably solve the so-called solar abundance problem without being excluded by terrestrial experiments

(e.g. LUX and XENON100) in which the scattering cross section is suppressed by the strong inverse dependence on q . The Sun is in fact an ideal DM detector for the type of particle considered here, since it measures the entire nuclear recoil energy spectra in the scatterings.

To summarize, in this work we have obtained two main results. Firstly, for the first time, a DM-baryon velocity dependent total cross-section has been implemented in solar simulation software. Secondly, but even more importantly, our analysis shows that DM particles with a mass of 10 GeV and a long-range interaction with ordinary matter mediated by a very light mediator (below roughly a few MeV), can have an impact on the Sun's sound speed profile without violating the constraints coming from direct DM searches. Our results are valid if the parameter k_χ which controls the self-interaction is of the order of k_χ^Ω . Larger values of this parameter, as we have shown in the last paragraph of Sec. 4, can dramatically reduced the effective luminosity carried by DM particles in the Sun and therefore our results can not be applied in that case. Furthermore, as commented upon in Sec. 5, it might well be possible that a dark sector with long-range forces can dissipate a relevant amount of energy through the emission of dark photons. A dissipative dark sector is extremely interesting because it can offer a rich array of new ideas ranging from the detection of primordial dark radiation to new possibilities for DM dynamics in virialized astrophysical objects.

We would like to thank Marco Taoso for useful discussions. This work was supported by grants from "Fundação para a Ciência e Tecnologia" and "Fundação Calouste Gulbenkian". This research has been supported at IAP by ERC project 267117 (DARK) hosted by Université Pierre et Marie Curie - Paris 6, and at JHU by NSF grant OIA-1124403.

REFERENCES

- Aalseth, C., Barbeau, P., Colaresi, J., Collar, J., Diaz Leon, J., et al. 2011a, *Phys.Rev.Lett.*, **107**, 141301
- Aalseth, C. et al. 2011b, *Phys.Rev.Lett.*, **106**, 131301
- Ade, P. et al. 2013, *arXiv.org*, 1303.5076
- Agnese, R. et al. 2013a, *arXiv.org*, 1304.4279
- 2013b, *Phys.Rev.*, **D88**, 031104
- Ahmed, Z. et al. 2010, *Science*, **327**, 1619
- Akerib, D. et al. 2013, *arXiv.org*, 1310.8214
- Angloher, G., Bauer, M., Bavykina, I., Bento, A., Bucci, C., et al. 2012, *Eur.Phys.J.*, **C72**, 1971
- Aprile, E. et al. 2011, *Phys.Rev.Lett.*, **107**, 131302
- Basu, S., Chaplin, W. J., Elsworth, Y., New, R., & Serenelli, A. M. 2009 *Astrophys.J.*, **699**, 1403
- Berezhiani, Z. 2005, *arXiv.org*, hep-ph/0508233
- Berezhiani, Z., Ciarelluti, P., Comelli, D., & Villante, F. L. 2005, *Int.J.Mod.Phys.*, **D14**, 107
- Berezhiani, Z., Comelli, D., & Villante, F. L. 2001, *Phys.Lett.*, **B503**, 362
- Bernabei, R. et al. 2008, *Eur.Phys.J.*, **C56**, 333
- 2010, *Eur.Phys.J.*, **C67**, 39
- Bertone, G., Hooper, D., & Silk, J. 2005, *Phys.Rept.*, **405**, 279
- Blinnikov, S. & Khlopov, M. Y. 1982, *Sov.J.Nucl.Phys.*, **36**, 472
- 1983, *Sov.Astron.*, **27**, 371
- Bovy, J. & Tremaine, S. 2012, *Astrophys.J.*, **756**, 89
- Busoni, G., De Simone, A., & Huang, W.-C. 2013, *JCAP*, **1307**, 010
- Casanellas, J. & Lopes, I. 2009, *Astrophys.J.*, **705**, 135
- 2013, *Astrophys.J.*, **765**, L21
- Catena, R. & Ullio, P. 2010, *JCAP*, **08**, 004
- Cirelli, M., Del Nobile, E., & Panci, P. 2013, *JCAP*, **1310**, 019
- Cumberbatch, D. T., Guzik, J., Silk, J., Watson, L. S., & West, S. M. 2010, *Phys.Rev.*, **D82**, 103503
- Kaplinghat, M., Tulin, S. & Yu, H. B. 2013, *arXiv*: 1308.0618
- de Blok, W. 2010, *Adv.Astron.*, **2010**, 789293
- Dehevels, S., Michel, E., Goupil, M., Marques, J., Mosser, B., et al. 2010, *A & A*, **514**, 31
- Essig, R., Jaros, J. A., Wester, W., Adrian, P. H., Andreas, S., et al. 2013, *arXiv.org*, 1311.0029
- Fan, J., Katz, A., Randall, L., & Reece, M. 2013a, *Phys.Rev.Lett.*, **110**, 211302
- 2013b, *Phys.Dark Univ.*, **2**, 139
- Fitzpatrick, A. L., Haxton, W., Katz, E., Lubbers, N., & Xu, Y. 2012, *JCAP*, **1302**, 004
- Foot, R. 2004a, *Phys.Rev.*, **D69**, 36001
- 2004b, *Int.J.Mod.Phys.*, **D13**, 2161
- 2008, *Phys.Rev.*, **D78**, 043529
- 2010, *Phys.Lett.*, **B692**, 65
- 2012, *Phys.Rev.*, **D86**, 023524
- Fornengo, N., Panci, P., & Regis, M. 2011, *Phys.Rev.*, **D84**, 115002
- Garbari, S., Liu, C., Read, J. I., & Lake, G. 2012, *MNRAS*, **425**, 1445
- Garrison-Kimmel, S., Rocha, M., Boylan-Kolchin, M., Bullock, J., & Lally, 2013, *MNRAS*, **433**, 3539
- Gates, E. I., Gyuk, G., & Turner, M. S. 1995, *Astrophys.J.*, **449**, L123
- 1996, *Phys.Rev.*, **D53**, 4138
- Gilliland, R. L., Faulkner, J., Press, W. H., & Spergel, D. N. 1986, *Astrophys.J.*, **306**, 703
- Gondolo, P., Edsjo, J., Ullio, P., Bergstrom, L., Schelke, M., et al. 2004, *JCAP*, **0407**, 008
- Gough, D. 2012, *Solar. Physics.*, **287**, 9-41
- Gould, A. 1987, *Astrophys.J.*, **321**, 571
- 1990, *Astrophys.J.*, **356**, 302
- Gould, A. & Raffelt, G. 1990, *Astrophys.J.*, **352**, 654
- Griest, K. & Seckel, D. 1987, *Nucl.Phys.*, **B283**, 681
- Guo, Q., White, S., Angulo, R. E., Henriques, B., Lemson, G., et al. 2013, *MNRAS*, **428**, 1351
- Guzik, J. A. & Mussack, K. 2010, *Astrophys.J.*, **713**, 1108
- Hamerly, R. & Kosovichev, A. G. 2012, *arXiv.org*, 1110.1169
- Hinshaw, G. et al. 2013, *Astrophys.J.Suppl.*, **208**, 19
- Kaplinghat, M., Tulin, S., & Yu, H.-B. 2013, *arXiv.org*, 1310.7945
- Kappl, R. & Winkler, M. W. 2011, *Nucl.Phys.*, **B850**, 505
- Klypin, A. A., Kravtsov, A. V., Valenzuela, O., & Prada, F. 1999, *Astrophys.J.*, **522**, 82
- Kobzarev, I., Okun, L., & Pomeranchuk, I. 1966, *Sov.J.Nucl.Phys.*, **3**, 837
- Kumar, J. & Learned, J.G. & Smith, S. & Richardson, K. 2012, *Phys.Rev.*, **D86**, 073002
- Lee, T. & Yang, C.-N. 1956, *Phys.Rev.*, **104**, 254
- Loeb, A. & Weiner, N. 2011, *Phys.Rev.Lett.*, **106**, 171302
- Lopes, I. 2013, *Phys.Rev.*, **D88**, 045006
- Lopes, I., Casanellas, J., & Eugenio, D. 2011, *Phys.Rev.*, **D83**, 63521
- Lopes, I., Kadota, K. & Silk, J. 2014, *Astrophys.J.*, **722**, L95
- Lopes, I. & Silk, J. 2002, *Phys.Rev.Lett.*, **88**, 151303
- 2010a, *Science*, **330**, 462
- 2010b, *Astrophys.J.*, **722**, L95
- 2012a, *Astrophys.J.*, **757**, 1301
- 2012b, *Astrophys.J.*, **752**, 129
- 2013, *MNRAS*, **435**, 21091
- Lopes, I. & Turck-Chieze, S. 2013, *Astrophys.J.*, **765**, 14
- Lopes, I. P., Silk, J., & Hansen, S. H. 2002, *MNRAS*, **331**, 361
- Lopes, I. P. & Gough, D., 2001, *MNRAS*, **322**, 473
- McCullough, M. & Randall, L. 2013, *JCAP*, **1310**, 058
- Morel, P. 1997, *A & A Supplement series*, **124**, 597
- Morel, P. & Lebreton, Y. 2008, *Astrophys.Space Sci.*, **316**, 611
- Navarro, J. F., Ludlow, A., Springel, V., Wang, J., Vogelsberger, M., et al. 2010, *MNRAS*, **402**, 21
- Panci, P. 2012, *arXiv.org*, 1206.2240
- Panci, P. 2014, *Adv.High Energy Phys.*, **2014**, 681312
- Petraki, K. & Volkas, R. R. 2013, *Int.J.Mod.Phys.*, **A28**, 1330028
- Rocha, M., Peter, A. H., Bullock, J. S., Kaplinghat, M., Garrison-Kimmel, S., et al. 2013, *MNRAS*, **430**, 81

- Salucci, P., Nesti, F., Gentile, G., & Martins, C. 2010, *A & A*, **523**, A83
- Scott, P., Fairbairn, M., & Edsjo, J. 2009, *MNRAS*, **394**, 82
- Scott, P., Venkatesan, A., Roebber, E., Gondolo, P., Pierpaoli, E., et al. 2011, *Astrophys.J.*, **742**, 129
- Serenelli, A., Basu, S., Ferguson, J. W., & Asplund, M. 2009, *Astrophys.J.*, **705**, L123
- Spergel, D. & Press, W. 1985, *Astrophys.J.*, **294**, 663
- Taoso, M., Iocco, F., Meynet, G., Bertone, G., & Eggenberger, P. 2010, *Phys.Rev.*, **D82**, 83509
- Tulin, S., Yu, H.-B., & Zurek, K. M. 2013, *Phys.Rev.*, **D87**, 115007
- Turck-Chieze, S., Basu, S., Brun, A. S., Christensen-Dalsgaard, J., Eff-Darwich, A., et al. 1997, *Solar Phys.*, **175**, 247
- Turck-Chieze, S. & Couvidat, S. 2011, *Rept.Prog.Phys.*, **74**, 086901
- Turck-Chieze, S. & Lopes, I. 1993, *Astrophys.J.*, **408**, 347
- . 2012, *Res.Astron.Astrophys.*, **12**, 1107
- Turck-Chieze, S., Palacios, A., Marques, J., & Nghiem, P. 2010, *Astrophys.J.*, **715**, 1539
- Vincent, A. C. & Scott, P. 2013, *arXiv.org*, 1311.2074
- Zentner, A. R. 2009, *Phys.Rev.*, **D80**, 063501
- Zentner, A. R. & Hearin, A. P. 2011, *Phys.Rev.*, **D84**, 101302